Environ Sci Pollut Res (2017) 24:16520–16530
DOI 10.1007/s11356-017-9213-0

RESEARCH ARTICLE

Novel highly porous magnetic hydrogel beads composed of chitosan and sodium citrate: an effective adsorbent for the removal of heavy metals from aqueous solutions

Shengyan Pu[1,2] · **Hui Ma**[1] · **Anatoly Zinchenko**[1,3] · **Wei Chu**[2]

Received: 15 November 2016 / Accepted: 7 May 2017 / Published online: 29 May 2017

Abstract This research focuses on the removal of heavy metal ions from aqueous solutions using magnetic chitosan hydrogel beads as a potential sorbent. Highly porous magnetic chitosan hydrogel (PMCH) beads were prepared by a combination of in situ co-precipitation and sodium citrate cross-linking. Fourier transform infrared spectroscopy indicated that the high sorption efficiency of metal cations is attributable to the hydroxyl, amino, and carboxyl groups in PMCH beads. Thermogravimetric analysis demonstrated that introducing Fe_3O_4 nanoparticles increases the thermal stability of the adsorbent. Laser confocal microscopy revealed highly uniform porous structure of the resultant PMCH beads, which contained a high moisture content (93%). Transmission electron microscopy micrographs showed that the Fe_3O_4 nanoparticles, with a mean diameter of 5 ± 2 nm, were well dispersed inside the chitosan beads. Batch adsorption experiments and adsorption kinetic analysis revealed that the adsorption process obeys a pseudo-second-order model. Isotherm data were satisfactorily described by the Langmuir equation, and the maximum adsorption capacity of the adsorbent was 84.02 mg/g. Energy-dispersive X-ray spectroscopy and X-ray photoelectron spectra analyses were performed to confirm the adsorption of Pb^{2+} and to identify the adsorption mechanism.

Keywords Magnetic chitosan beads · Porous structure · Heavy metal · Bioadsorbent

S. Pu and H. Ma. contributed equally to this work.

Responsible editor: Guilherme L. Dotto

Electronic supplementary material The online version of this article (doi:10.1007/s11356-017-9213-0) contains supplementary material, which is available to authorized users.

✉ Shengyan Pu
pushengyan@gmail.com

✉ Anatoly Zinchenko
zinchenko@urban.env.nagoya-u.ac.jp

[1] State Key Laboratory of Geohazard Prevention and Geoenvironment Protection, Chengdu University of Technology, 1#, Dongsanlu, Erxianqiao, Chengdu 610059, Sichuan, People's Republic of China

[2] Department of Civil and Environmental Engineering, The Hong Kong Polytechnic University, Hong Kong, People's Republic of China

[3] Graduate School of Environmental Studies, Nagoya University, Nagoya 464-8601, Japan

Introduction

Currently, the contamination of water by heavy metal ions has drawn global attention due to their nondegradability (Jarup 2003). The bioconcentration of heavy metal ions through the food chain makes the problem an intractable threat to human health (Lin et al. 2016). Many research groups have devoted efforts to find suitable materials as adsorbents for the purification of wastewater contaminated with heavy metals (Zhou et al. 2009). To avoid secondary pollution and reduce costs, renewable biomaterials with robust absorbability have gained increased attention (Singh et al. 2003). Due to its abundant natural occurrence, chitin has attracted great attention from researchers. Chitosan, a commercially available derivative of chitin with more reactive functional groups (typical commercial chitosan has 66–99% degree of deacetylation), is one of the most potential starting materials (Varma et al. 2004). Thus, it has broad application prospects in the field of wastewater purification (Li et al. 2016a).

In a number of previous reports, adsorbents based on chitosan have shown good adsorption capacity (Prakash et al.

2012). Chitosan-based hydrogel beads, such as poly(methacrylic acid)-grafted chitosan microspheres (Huang et al. 2013), impregnated chitosan beads (Wang et al. 2014), and acrylic acid-grafted alginate/chitosan beads(Abou El Fadl 2014), were reported to adsorb heavy metal ions. To obtain more effective treatment, amino and hydroxyl groups, the main functional groups of chitosan that effectively chelate a broad range of metal ions, have to be accessible during the adsorption process (Dinu and Dragan 2010; Ngah and Fatinathan 2010). The research on chitosan-based adsorbents has utilized two dominating systems to achieve this goal: (1) porous chitosan hydrogel (Liu et al. 2010; Wang and Chen 2014; Lin et al. 2017) and (2) chitosan nanoparticles (Hosseini et al. 2016; Lu et al. 2016). Chitosan hydrogels satisfy this requirement due to their porous structure, but the difficulty in separating the metal ions and the low diffusion velocities in a bulk hydrogel limit their applications (Li et al. 2016b). Magnetic separation has been a promising environmental purification technique because it produces no contaminants during treatment and can treat a large amount of wastewater within a short time (Men et al. 2012; Kharissova et al. 2015). Magnetic chitosan-based hydrogels, such as magnetic chitosan/cellulose microspheres (Luo et al. 2015), ethylenediamine-modified cross-linked magnetic chitosan resin (Hu et al. 2011), and PVA/chitosan magnetic composite (Zhu et al. 2014), were reported to adsorb heavy metal ions. Decreasing the size of the elementary unit of the adsorbent to fabricate magnetic nanoparticles is another approach to overcome these drawbacks (Chen et al. 2014; Galhoum et al. 2015). The utilization of magnetite-bonded chitosan particles (Kim et al. 2016) or hybrid materials containing magnetite particles (Podzus et al. 2009) is a feasible option to facilitate the recycling process of chitosan-based materials. Contaminants can be absorbed using magnetic adsorbents and then separated from a solution by using an external magnetic field. Various approaches have been developed for preparing magnetic chitosan microspheres or nanoparticles; however, the preparation process of chitosan-Fe_3O_4 nanoparticles is quite complicated and requires multistep operations and harsh reaction conditions (Hritcu et al. 2011; Jiang et al. 2014). Additionally, the use of emulsifiers and surfactants in previous methods to prevent the coagulation of the adsorbent particles in solution resulted in substantial environmental contamination. In recent years, application of the chelating function of chitosan to immobilize the Fe^{2+}/Fe^{3+} and then to co-precipitate Fe_3O_4 particles or Fe_3O_4-bonded chitosan particles has been reported (Li et al. 2006). However, to obtain the nanoscale Fe_3O_4-bonded chitosan particles by these methods (Li et al. 2006; Wang et al. 2009), the excess chitosan has to be washed off, which imposes higher manufacturing costs and unnecessary waste (Yuwei and Jianlong 2011). Therefore, combining the advantages of magnetic chitosan nanoparticles and chitosan hydrogels, the adsorbent based on chitosan hydrogel beads and containing magnetic particles (Mi et al. 2015), which can provide enough contact area during the adsorption process, would be an ideal solution to solve the above problems.

Herein, we describe the advantages of using both chitosan hydrogel and magnetic chitosan nanoparticles to fabricate a novel magnetic adsorbent by a facile one-step in situ co-precipitation process. Batches of the adsorption experiments were performed systematically. During the fabrication process, nontoxic reagents were used, which completely eradicated the secondary contamination. The main characteristics of the porous magnetic chitosan hydrogel (PMCH) beads are (1) uniform porous structure, (2) multilayer structure, and (3) controlled size. Such structures can be utilized to respond to different demands under particular conditions.

Materials and methods

Materials

Chitosan (95% deacetylation, viscosity average molecular weight 3.0×10^5 g mol^{-1}) was obtained from Aladdin Reagent Factory (Shanghai, China). Acetic acid, sodium hydroxide, and sodium citrate were purchased from Kelong Chemical Reagent Factory (Chengdu, China). $FeCl_3 \cdot 6H_2O$, $FeCl_2 \cdot 4H_2O$, and $Pb(NO_3)_2$ were obtained from Zhiyuan Chemical Reagent Factory (Tianjin, China). All compounds are commercially available chemicals and were used as received without further purification. Deionized water used for all experiments was generated from the Milli-Q water purification system (Ulupure Corporation).

Methods

Preparation of stock solution

The Fe^{3+}/Fe^{2+} mixture solution (molar ratio = 2) was prepared by dissolving 2.956 g of $FeCl_3 \cdot 6H_2O$ and 1.087 g of $FeCl_2 \cdot 4H_2O$ in 12.5 mL ultra-pure water. The alkaline soaking solution was prepared by dissolving 12.500 g of sodium hydroxide and 7.356 g of sodium citrate into 250 mL ultra-pure water.

Preparation of PMCH beads

First, 0.8 g chitosan was dissolved in 24 mL 2.0% acetic acid solution and stirred for 30 min at 3000 r/min. Next, 2 mL Fe^{3+}/Fe^{2+} solution was added to the chitosan solution and stirred for another 30 min. The color of the resulting viscous solution changed from intense yellow to dark red. Subsequently, the composite sol was slowly dropped into an alkaline solution of sodium citrate by a peristaltic pump through a tube with an

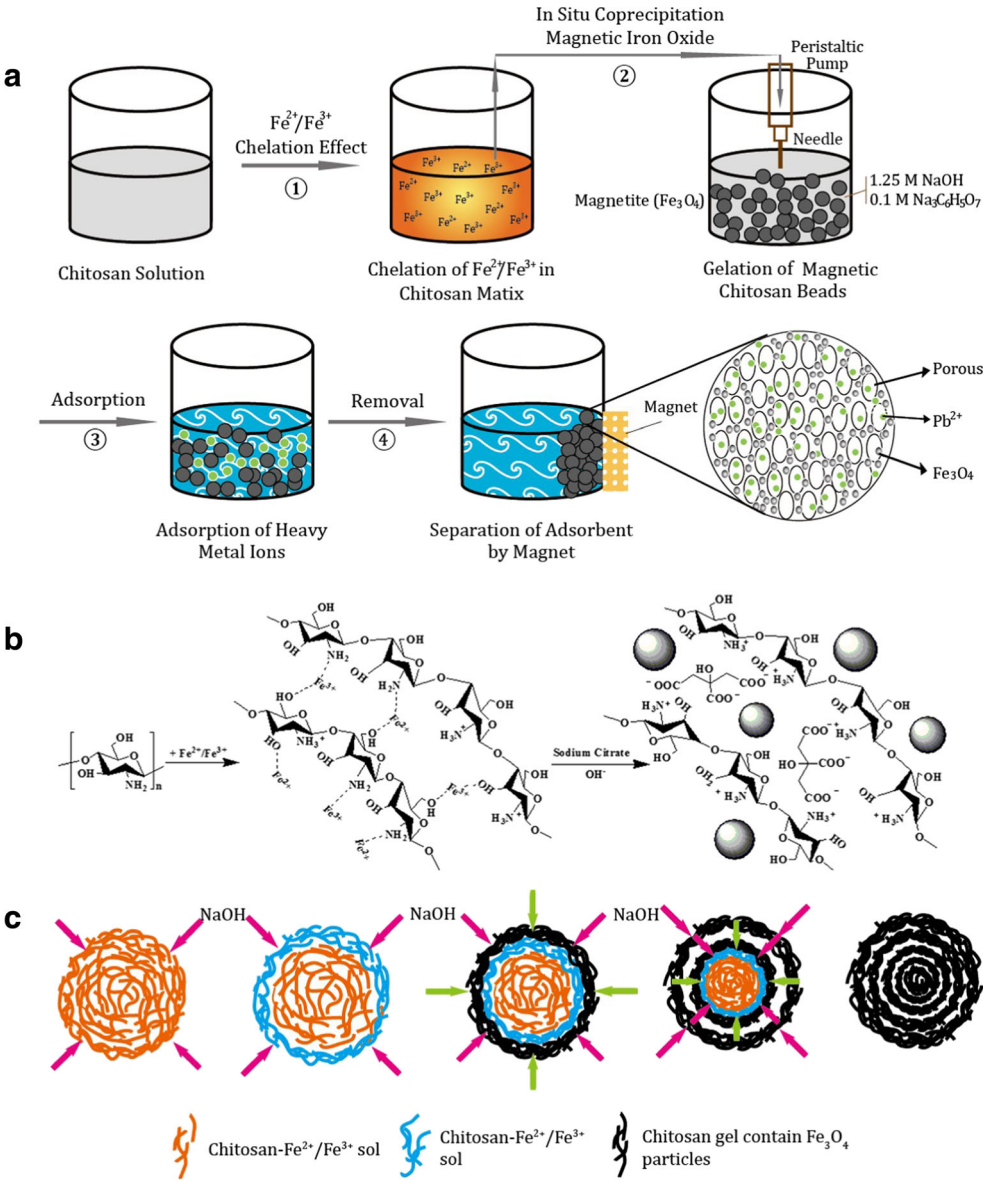

Fig. 1 **a** Schematic illustration of preparation of PMCH beads and removal of heavy metal ions from aqueous solution. **b** Fe^{2+} and Fe^{3+} ion complex with chitosan and Fe_3O_4 particles are formed. **c** The magnetic hydrogel beads are formed along with the diffusion of alkaline solution. The stepwise layer-by-layer shrinking of the gel results in the formation of a multilayer structure

inner diameter of 0.4 mm and soaked for 24 h. After that step, the formed beads were extensively washed several times with a diluted hydrochloric acid solution and deionized water to remove the residual alkali and cross-linker.

Batch adsorption experiments

A 200 mg/L Pb^{2+} solution was prepared by dissolving 0.320 g lead nitrate in 1 L ultra-pure water. In the adsorption experiment, 2.000 g wet PMCH beads was added to a conical flask (150 mL) containing 40 mL Pb^{2+} solution and shaken at 160 r/min at room temperature for 24 h. After separation of the adsorbent by an external magnet, the final concentration of Pb^{2+} was analyzed by an atomic absorption spectrophotometer (Ggx-9, Haiguang, Beijing). The degree of adsorption (q) was calculated by the following equation:

$$q = (C_0 - C_t)V/M$$

where C_0 and C_t are the concentrations of Pb^{2+}solution (mg/L) before and after adsorbing for t min, respectively, V is the volume of the Pb^{2+} solution, and M is the weight of magnetic adsorbent. All experiments were repeated in triplicate, and the average of three replicate experiments was calculated and used for data analysis.

Desorption of heavy metals and reusability of PMCH beads

After adsorption of lead from 40 mL of 200 mg/L Pb^{2+} solution, the adsorbent was separated by an external magnet and

then mixed with 20 mL 0.01 M ethylenediaminetetraacetic acid disodium (Na_2EDTA) solution under stirring for 5 min, then washed several times with deionized water to remove extra desorption solution. The composite microspheres were then exposed in Pb^{2+} solution under the same conditions. Five consecutive cycles of adsorption-desorption were executed to test the reusability of the adsorbent.

Results and discussion

Preparation of PMCH beads

We employed chitosan and iron salts as the components for the in situ co-precipitation reaction and sodium citrate as a cross-linker to fabricate the multilayered PMCH beads and remove Pb^{2+}at room temperature. As shown in Fig. 1, Fe^{2+}/Fe^{3+} solution was added to the chitosan/acetic acid solution, and Fe^{2+}/Fe^{3+} chelated with the chitosan matrix. Then, the mixed solution was dropped into the alkaline solution and soaked for 24 h, where Fe_3O_4 was generated by in situ co-precipitation and chitosan was cross-linked with citrate ions. Subsequently, heavy metal ions were adsorbed on the functional groups of PMCH beads, and the adsorbent was separated by an external magnet.

The basic principle of the PMCH bead formation process is illustrated in Fig. 1b, c. PMCH beads were formed by chelating Fe^{2+} and Fe^{3+} ions with chitosan followed by formation of Fe_3O_4 through the in situ co-precipitation reaction and cross-linking of chitosan with citrate ions (Fig. 1b). The magnetic chitosan beads were fabricated by dropping the resulted reaction mixture into the soaking solution. The gel and Fe_3O_4 nanoparticles (NPs) were formed immediately when the sol contacted the alkaline solution, more rapidly than the OH^- diffusion velocity. Diffusion of the OH^- and the existence of Fe_3O_4 NPs resulted in layer-by-layer shrinking and the eventual formation of a multilayer structure (Fig. 1c).

Photographic images of wet and dried PMCH beads in Fig. 2 (a, b) show a dramatic shrinkage of beads because of dehydration (drying). As shown in Fig. 2 (c), after an external magnet is placed beside a solution with beads, the hydrogel beads are separated from the solution, and thus the beads can be recycled and reused easily after the adsorption step. And on this foundation, with the way of observation, it is visual to have compared the difference of pure chitosan gel beads and magnetic chitosan beads (see Supporting Information, Fig. S1). To address particular application demands, the size of composite beads can be controlled in a range between 0.1 and 20 mm (Fig. 2 (d)) by adjusting the drop size in the dropping process. To observe the interior structure of the beads, a PMCH bead with 20 mm diameter was cut in half, and the multilayer onion-like structure was clearly observed (Fig. 2 (d′)). The particle size distributions of the beads before and after drying are shown in Fig. 2 (e). The average volume

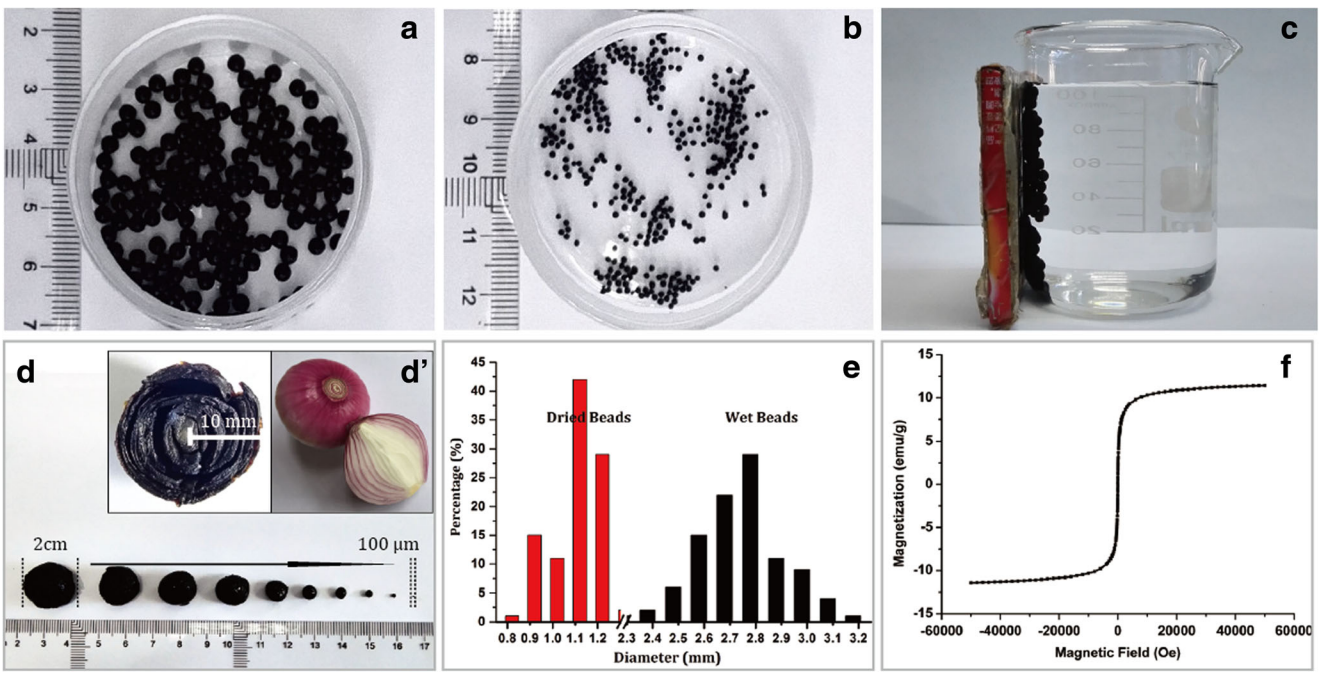

Fig. 2 Photographic images of *a* wet and *b* dried magnetic chitosan hydrogel beads. *c* Magnetic chitosan hydrogel beads collected by an external magnet. *d* Size-controlled magnetic hydrogel beads of 0.1 mm to 2.0 cm diameters. *d′* The onion-like multilayered cross-sectional structure of wet PMCH beads. *e* Diameter distributions of wet and dried hydrogel beads. At least 100 beads were measured to build each distribution. *f* Hysteresis loop of PMCH beads in the range of −60000–60000 Oe

of the microspheres decreased by approximately 15 times, yet the spherical shape of the beads was retained. The moisture content of the hydrogel beads measured by an electronic rapid moisture analyzer was approximately 93%, which is consistent with the above volume decrease.

The magnetic hysteresis loop of the PMCH beads is shown in Fig. 2 (f). The saturation magnetization of the PMCH beads was 11.3 emu/g, which revealed that magnetic beads can be recycled by using an external magnet. It also confirms the existence of Fe_3O_4 by correspondence with other characterization results.

Microscopic characterization

To identify the functional groups in the resultant hydrogel beads, Fourier transform infrared spectroscopy (FTIR) spectra of (a) pure chitosan, (b) the PMCH beads, and (c) the PMCH beads after exposure to Pb^{2+} ion solution were analyzed (Fig. 3). The interaction between chitosan, citrate, and Pb^{2+} affects the position and the intensity of characteristic peaks. Pure chitosan hydrogel beads are characterized by a peak located at 1074 cm^{-1} attributed to the C–O stretching mode of the CH_2–OH group (Reddy and Lee 2013), a peak at 1382 cm^{-1} related to the –C–O stretching of the primary alcohol group (Hritcu et al. 2011), and a peak at 1419 cm^{-1} attributed to the C–N stretching (Fig. 3a, sample a). The band at 1594 cm^{-1} is assigned to the C═O bending vibration, and the peak at 1643 cm^{-1} is assigned to the N–H stretching (Peng et al. 2014). The broad absorption peak at 3430 cm^{-1} corresponds to –OH and $–NH_2$ stretching vibrations (Wang et al. 2008).

The intrinsic peaks remain in both spectra of the magnetic hydrogel beads. The peak that appeared at 574 cm^{-1} in samples b and c is attributed to the Fe–O bond vibration, which is the characteristic absorption peak for Fe_3O_4 (Peng et al. 2014). In the spectrum of sample b, the intensity of the amide peak at 1643 cm^{-1} decreased, while the intensity of the C═O peak at 1594 cm^{-1} increased as a result of cross-linking by citrate and weak interactions between Fe_3O_4 and chitosan. Peaks at 1643 and 1598 cm^{-1} combined together in Fig. 3a (sample c), suggesting complex formation between Pb^{2+} ions and chitosan.

Thermal methods, such as thermogravimetry (TG) and differential thermogravimetry (DTG), have been used as powerful tools to interpret physical and chemical changes in both natural and synthetic polymers (Giacometti et al. 2005). The TG and DTG curves both of pure chitosan beads and of magnetic chitosan beads are shown in Fig. 3b, c. Figure 3b shows that the weight loss of pure chitosan beads occurred in three stages. First, bound water was lost in the range 25–90 °C, which is an endothermic process (Fig. 3c). In the second stage, the chitosan decomposed in the temperature range of 90–320 °C. The peak at 300 °C indicates that the decomposition velocity is fast at 300 °C. When the temperature increased further, the weight slowly declined. The weight at 800 °C corresponded to the residual carbon, which is the final product of pyrolysis. In the case of the PMCH beads, the bound water

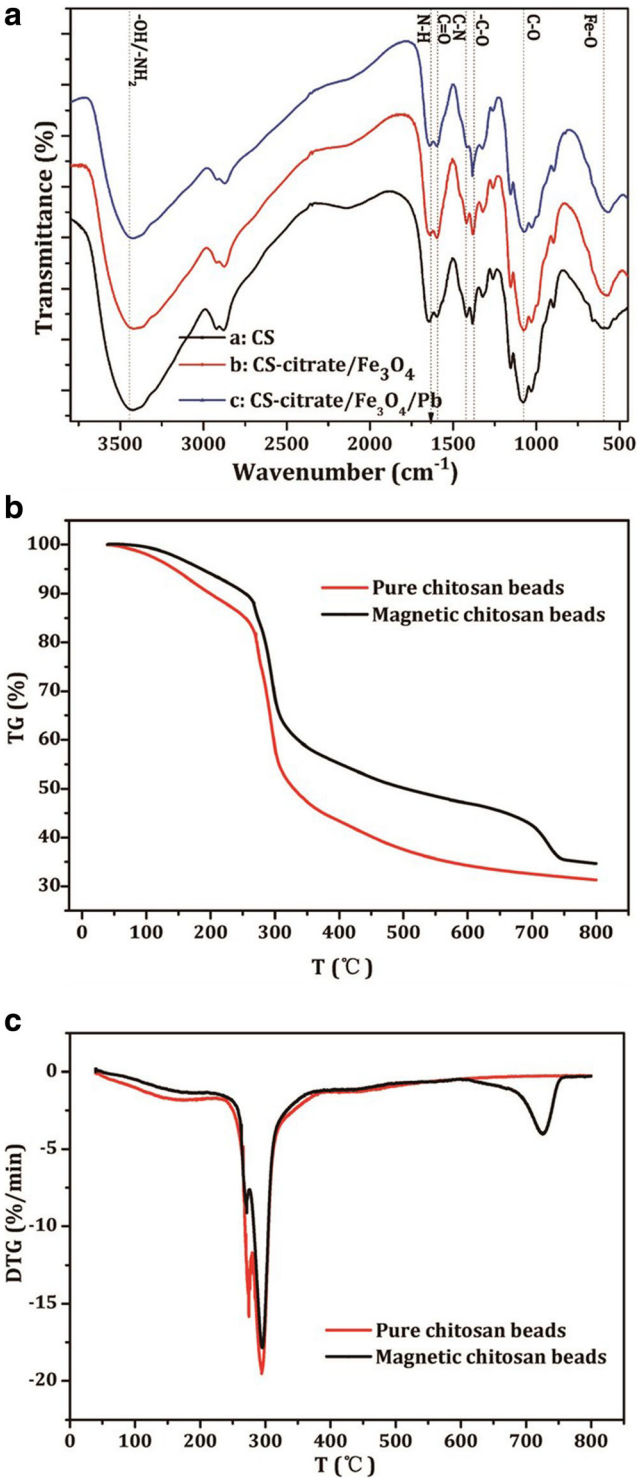

Fig. 3 **a** FTIR spectra of *a* pure chitosan beads and PMCH beads *b* before and *c* after adsorption of Pb^{2+}. **b** The weight loss of the pure chitosan beads and the PMCH beads with the increase of temperature. **c** Differential DTG curves of pure chitosan beads and the magnetic chitosan beads

was eliminated in the range of 25–120 °C accompanied by an adsorption of heat, and the chitosan decomposed completely at 320 °C. The third stage involved the carbonization of decomposed chitosan. Then, at ca. 600 °C, Fe_3O_4 reacted with the carbon to generate monoplasmatic iron, and the reaction rate reached its maximum at 710 °C and ended at 750 °C. The residual weight at 800 °C corresponded to the carbon and the monoplasmatic iron. The decomposition onset temperature of the PMCH beads is higher than for pure chitosan beads, which indicated that the existence of Fe_3O_4 increased the thermal stability of the adsorbent, but the introduction of Fe_3O_4 NPs did not prevent the degradability of the adsorbent. The adsorbent can still be easily degenerated after lose efficacy.

Confocal microscopy was used to analyze the interior structure of the adsorbent. The sectional images of pure chitosan beads and PMCH beads are shown in Fig. 4. Pure chitosan beads have a smooth sectional view (Fig. 4 (a)), but in the sectional profile of magnetic beads, the concentric rings are indicative of a multilayered structure (Fig. 4 (b)). Furthermore, in the magnified micrographs, pure chitosan beads show no characteristic features (Fig. 4 (c)), while the porous structure of the magnetic chitosan gel beads can be clearly observed in Fig. 4 (d), which has pores with an average diameter of 12 μm. A piece of the PMCH beads from the inside and analyzed by SEM, the highly porous structure, and the multilayer structure were observed (see Supporting Information, Fig. S2). The large surface area of this highly porous material can provide a large contact area for adsorption processes.

TEM observation was performed to gain deeper insight into the nanoscale morphology of PMCH beads containing Fe_3O_4 nanoparticles (Fig. 4 (e)). Fe_3O_4 NPs were well dispersed in PMCH beads due to their homogeneous growth. The corresponding size distribution of Fe_3O_4 NPs is shown in Fig. 4 (e'); the diameter of Fe_3O_4 NPs is 5 ± 2 nm. EDS spectra of PMCH beads before and after Pb^{2+} adsorption are shown in Fig. 4 (f). The peaks of C and O indicate major constituents of chitosan. The intense peaks at 0.7 and 6.4 keV indicate the presence of Fe as a part of Fe_3O_4. The EDS spectra of PMCH beads after adsorbing Pb^{2+} contain new peaks (Fig. 4 (f')), and intense peaks at 1.8 and 2.3 keV indicate the presence of Pb^{2+}. The EDS spectra provide direct evidence for the efficient adsorption of Pb^{2+} by PMCH beads.

Figure 5a–c shows XPS spectra of pure chitosan beads and PMCH beads before and after Pb^{2+} adsorption. Compared with Fig. 5a, the new peak with binding energy (BE) of 720 eV appeared in Fig. 5b, c. The Fe 2p BE signal has a low intensity due to a low atomic content, but in the result of EDS shown in Fig. 4 (f), the element Fe was detected. In the FTIR spectrum in Fig. 3a, the peak at 574 cm^{-1} is attributed to

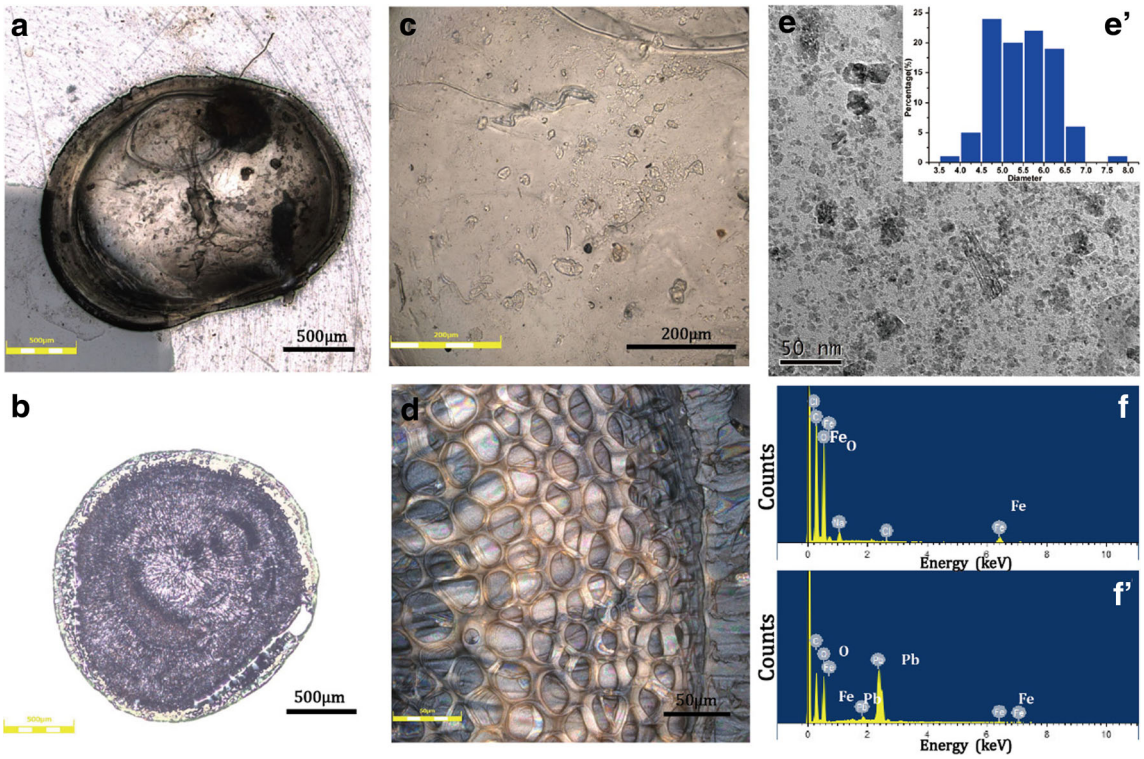

Fig. 4 Laser confocal scanning microscopy images of *a* the section and *c* the magnified interior structure of pure chitosan beads. *b* The sectional view and multilayer structure of PMCH beads, and *d* the magnified porous structure of PMCH beads. *e* TEM image of the inner part of PMCH beads; Fe_3O_4 NPs are well dispersed in the chitosan matrix. *e'* Size distribution of Fe_3O_4 NPs inside PMCH beads. EDS spectra of the PMCH beads *F* before and *F'* after adsorption of Pb^{2+}

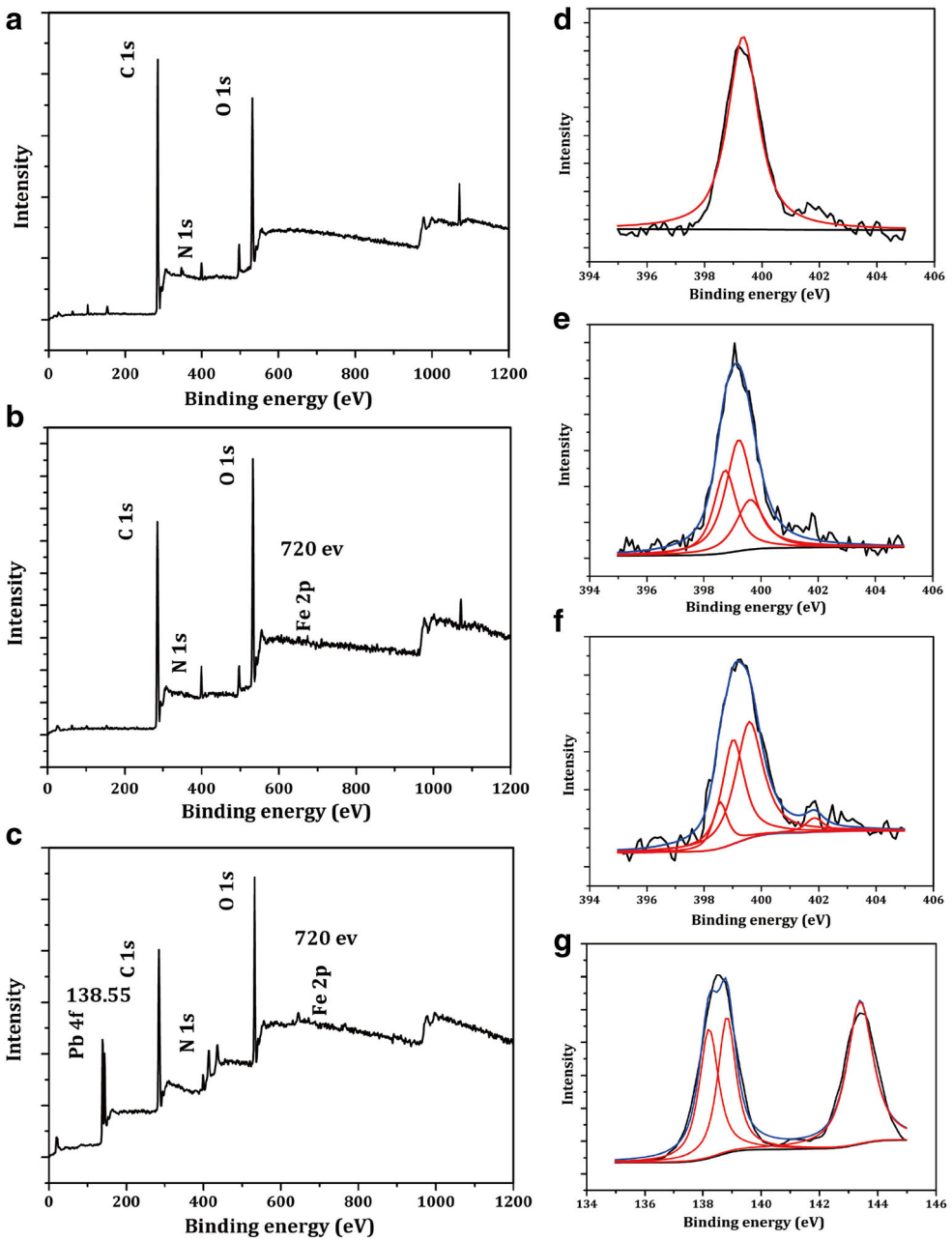

Fig. 5 XPS spectra of **a** pure chitosan beads and PMCH beads **b** before and **c** after adsorbing Pb^{2+}. N 1s spectra of **d** pure chitosan, **e** PMCH beads, and **f** PMCH beads after adsorbing Pb^{2+}. **g** The Pb spectra in the resulting PMCH beads

Fe–O bond vibration. The combined results of EDS, FTIR, and XPS confirm the existence of Fe. The Pb 4f peak with binding energy of 138.55 eV appeared in Fig. 5c as a result of the Pb^{2+} adsorption process. The O 1s signal in Fig. 5a–c did not change, which might indicate that hydroxyl groups of chitosan do not play a major role in the chemical binding of Pb^{2+} during adsorption. However, the N 1s signal shifted due to cross-linking and the weak interaction between the Fe_3O_4 particles and chitosan (Wang et al. 2011) (Fig. 5d, e). Furthermore, the N 1s peak at 401.8 eV can be observed (He et al. 2014), which may indicate that a pair of electrons in the nitrogen atom was donated to form a coordination bond between N and Pb^{2+} (Peng et al. 2014) (Fig. 5f).

Adsorption of heavy metal by PMCH beads

Heavy metal ion adsorption experiments (specifically Pb(II)) were performed to evaluate the influence of key parameters such as solution pH and adsorption time.

The pH values selected in this experiment ranged from 3 to 6 and were adjusted by adding 1 M hydrochloric acid solution. As shown in Fig. 6a, the uptake capacity of Pb^{2+} increased with increasing pH, and the maximum adsorption amount (45.2 mg/g) was achieved at pH 6. This may be because the $–NH_2$ groups are protonated at low pH values, which is unfavorable for the adsorption of Pb^{2+} due to the electrostatic repulsion and inability of Pb^{2+} and

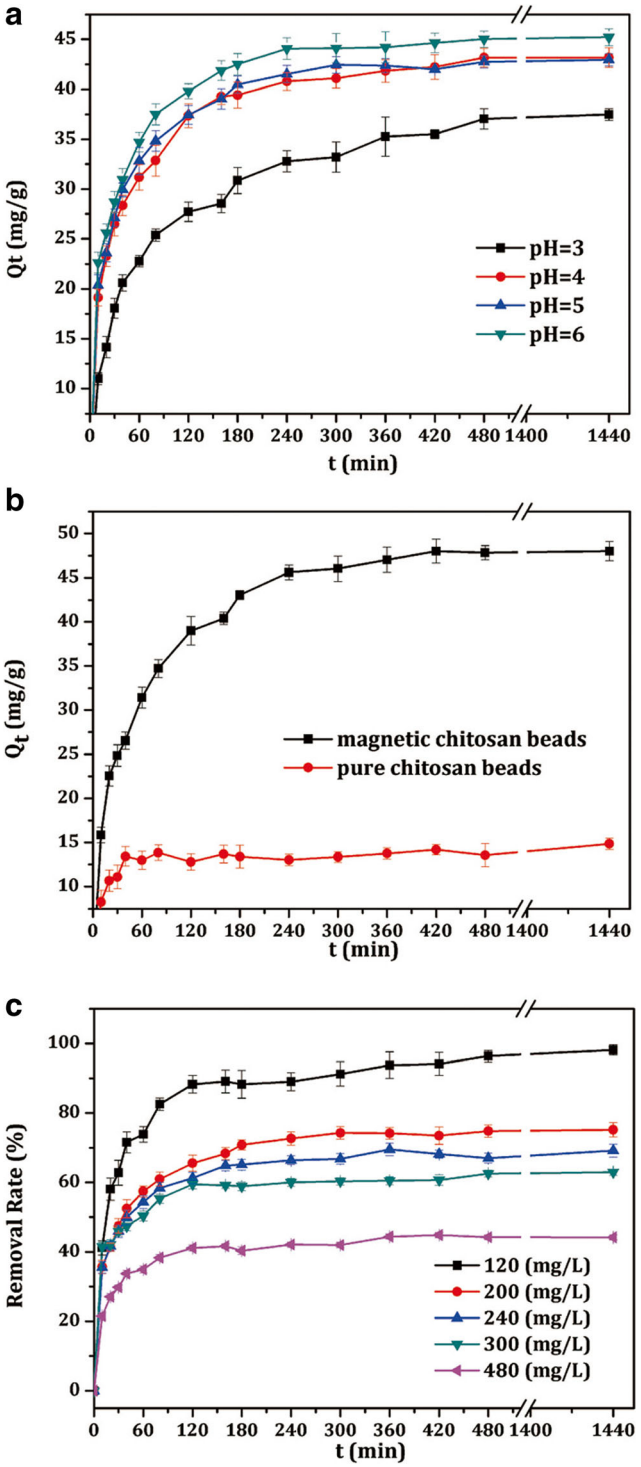

Fig. 6 **a** Amount of Pb^{2+} adsorbed by the PMCH beads under varied pH values (pH = 3, 4, 5, 6; initial concentration 200 mg/L). **b** Relative amount of Pb^{2+} adsorbed by the PMCH beads and the pure chitosan beads at different times under the same experimental conditions (pH = 6; initial concentration 200 mg/L). **c** The Pb^{2+} removal efficiency of the magnetic chitosan beads with different initial concentrations (pH = 6; initial concentrations: 120, 200, 240, 300, 480 mg/L)

the nitrogen of the amine group to form a coordination bond (Guibal et al. 2004).

Adsorption time is an important parameter that can affect the adsorption kinetics. Figure 6b shows that the amount of Pb^{2+} adsorbed by PMCH beads increased with the increase of adsorption time. The adsorption capacity of magnetic beads is significantly higher than that of pure chitosan beads because the highly porous structure of the magnetic composite provides a large specific surface area, which leads to higher adsorption of Pb^{2+} compared to the pure chitosan beads. The adsorbed amount of Pb^{2+} by magnetic bead adsorbent increased sharply during the first 180 min. Then, the rate slowed down, and the adsorption reached an equilibrium value after approximately 24 h. The extended adsorption kinetics might reflect the porous structure of PMCH beads. In the beginning of the adsorption process, the adsorbate diffuses quickly into the adsorbent, and the adsorption sites are easily accessed by Pb^{2+} ions. Later, however, during the adsorption process, more active sites were occupied, and the remaining active sites are not easily accessed.

The adsorption experiments were performed at different initial Pb^{2+} concentrations ranging from 120 to 480 mg/L at pH 5.0, and kinetic curves were measured over 24 h adsorption time. The removal efficiency decreased slightly with the increase of Pb^{2+}concentration, as shown in Fig. 6c, but the removal amounts increased with greater concentrations.

Adsorption kinetics

The adsorption process on porous adsorbents mainly follows three steps: (1) diffusion of adsorbates toward the external surface of adsorbent, (2) diffusion of adsorbates into the pores of adsorbent, and (3) adsorption of adsorbates on the internal surface of the adsorbent (Ruthven 1984). To reveal the mechanism that controls the adsorption process, three kinetic models, i.e., the pseudo-first-order model, pseudo-second-order model, and intraparticle diffusion model, were employed to analyze the adsorption kinetics (Jeon et al. 2004).

The results of the kinetic analysis are shown in Table 1 (see Supporting Information, kinetic equations, and Fig. S3). The pseudo-second-order equation represented the adsorption process best, suggesting that the overall adsorption process is controlled by chemisorptions, in which specific surface area is a significant factor affecting the adsorption.

Table 1 Best-fit kinetic model parameters for Pb^{2+} adsorption on magnetic chitosan beads

	Q_e (mg/g)	k	R^2
First-order model	$q_{e(cal)}$ (mg/g) = 18.81	k_1 (min^{-1}) = 0.00932	0.9629
Second-order model	$q_{e(cal)}$ (mg/g) = 45.81	k_2 (g/(mg min)) = 0.00149	0.9998
Intraparticle model	–	k_p (mg/g $min^{0.5}$) = 0.67202	0.5828

Table 2 Best-fit isotherm model parameters for Pb^{2+} adsorption on magnetic chitosan beads

Langmuir		Freundlich	
q_m (mg/g)	84.02	K_F (mg/g)	20.54
b	0.0669	n	4.142
R^2	0.9333	R^2	0.8536

Isothermal adsorption

To quantify the adsorption capacity of the PMCH beads, the Langmuir and Freundlich adsorption isotherm models were used to interpret the adsorption data.

The Langmuir equation is represented as

$$\frac{C_e}{q_e} = \frac{1}{bq_m} + \frac{C_e}{q_m}$$

where q_e (mg/g) and C_e (mg/L) represent the amount of adsorbed adsorbate and its concentration in solution at equilibrium, b (L/mg) is the Langmuir adsorption equilibrium constant, and q_m (mg/g) is the maximum adsorption capacity for monolayer formation on an adsorbent.

The Freundlich isotherm is an empirical equation used to describe heterogeneous systems, and it is expressed as

$$\ln q_e = \ln K_F + \frac{1}{n} C_e$$

where K_F is the Freundlich constant, and n is the heterogeneity factor.

The theoretical parameters of adsorption isotherms along with regression coefficients are summarized in Table 2 (see Supporting Information, Fig. S4). For the two isotherm models we studied, the data fit the Langmuir model better than the Freundlich model, suggesting that the maximum adsorption capacity of magnetic beads is 83.40 mg/g. It has been reported that values of n in the range 1–10 represent good adsorption (Bulut et al. 2007). In the present work, the exponent was $1 < n < 10$, indicating the adsorption system is "favorable."

Table 3 compares the adsorption capacities of chitosan-based adsorbent with different types of adsorbents previously used for the removal of heavy metals. The maximum adsorption capacity of Pb^{2+} on PMCH beads was higher than that of other previously reported adsorbents, indicating that PMCH beads prepared by a combination of in situ co-precipitation and sodium citrate cross-linking were an efficient adsorbing material for the removal of heavy metals from aqueous solutions.

Table 3 The comparison of magnetic chitosan beads with other chitosan-based adsorbents

Adsorbent	Adsorbate	Q_{max} (mg/g)	Reference
Magnetic chitosan beads	Arsenic(V) Arsenic(III)	35.7 35.3	(Wang et al. 2014)
Epichlorohydrin-crosslinked chitosan particle	Copper(II) Zinc(II) Lead(II)	35.46 10.21 34.13	(Chen et al. 2008)
Chitosan-bound Fe_3O_4 nanoparticles	Copper(II)	21.5	(Chang and Chen 2005)
Magnetic chitosan/cellulose microspheres	Cadmium(II) Lead(II)	61.12 45.86	(Luo et al. 2015)
Poly(methacrylic acid)-chitosan microspheres	Copper(II)	83.2	(Huang et al. 2013)
PVA/chitosan magnetic composite	Cobalt(II)	14.39	(Zhu et al. 2014)
Ethylenediamine-magnetic chitosan resin	Chromium(VI)	51.813	(Hu et al. 2011)
Magnetic chitosan beads	Lead(II)	84.02	This study

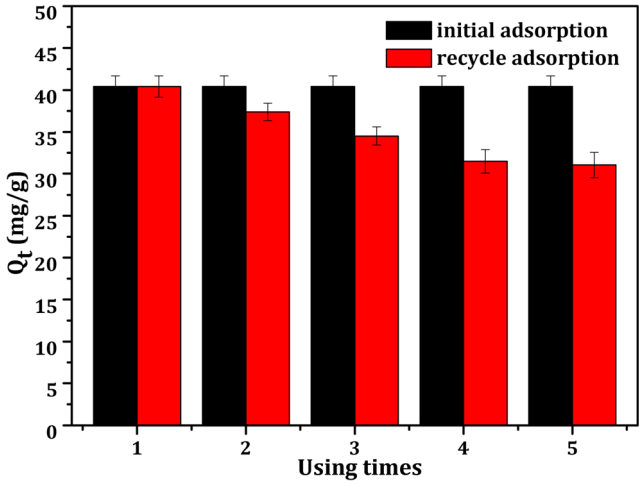

Fig. 7 Adsorption capacity of PMCH bead adsorbent for Pb^{2+} during cyclic experiments (40 mL Pb^{2+} solution with initial concentration of 200 mg/L at pH 5.0)

Desorption experiment

The regeneration ability is an important property for evaluating the potential application value of a bioadsorbent. As shown in Fig. 7, the adsorption capacity for Pb^{2+} has a small decrease after 5 cycles.

The complexing capacity of the ethylenediaminetetraacetic acid disodium (Na_2EDTA) is stronger than that of chitosan (Ge et al. 2016), so Pb^{2+} was complexed by Na_2EDTA, and the active functional groups were released. Therefore, the reuse study of adsorbent indicated that PMCH beads were an efficient and stable adsorbent for Pb^{2+} removal. Though the adsorption property of the magnetic gel beads decreased somewhat after 5 cycles, the adsorption result was not affected significantly in the purification of wastewater containing low concentration of heavy metals. However, for high concentrations of the pollutants in wastewater, the recycling rate may need to be enhanced further.

Conclusions

In this research, porous magnetic chitosan hydrogel (PMCH) beads were prepared by in situ co-precipitation and sodium citrate cross-linking using no toxic reagents. The structure and heavy metal adsorption properties of the porous magnetic chitosan hydrogel beads were thoroughly investigated. PMCH beads showed a great affinity for heavy metal ions, such as Pb^{2+}, due to the presence of efficient chelating amino groups and a large specific area. The maximum adsorption capacity for Pb^{2+} reached 84.02 mg/g. The kinetics of adsorption was best described by the pseudo-second-order kinetic model, and the adsorption equilibrium was well approximated by Langmuir adsorption isotherms. Overall, PMCH was shown to be a bioadsorbent with excellent adsorption capacity that can be easily recovered after the treatment of wastewater containing heavy metal ions. This novel multilayer porous magnetic adsorbent fabricated by an environmentally friendly and facile method represents a low-cost alternative to other adsorbents. Because of the advantages and special structure of the adsorbent, these results might inspire other applications in further research.

Acknowledgments This work was supported by the National Natural Science Foundation of China (51408074) and the Research Fund of State Key Laboratory of Geohazard Prevention and Geoenvironment Protection (Nos. SKLGP2015Z007, SKLGP2017Z009). Dr. Shengyan PU is grateful for the support from the Hong Kong Scholars Program (No. XJ2015005 and G-YZ80) and the Project Funded by China Postdoctoral Science Foundation (2015T80966).

Compliance with ethical standards

Conflict of interest The authors declare that there is no conflict of interest.

References

Abou El Fadl FI (2014) Radiation grafting of ionically crosslinked alginate/chitosan beads with acrylic acid for lead sorption. J Radioanal Nucl Chem 301:529–535

Bulut Y, Gözübenli N, Aydın H (2007) Equilibrium and kinetics studies for adsorption of direct blue 71 from aqueous solution by wheat shells. J Hazard Mater 144:300–306

Chang YC, Chen DH (2005) Preparation and adsorption properties of monodisperse chitosan-bound Fe3O4 magnetic nanoparticles for removal of Cu(II) ions. J Colloid Interface Sci 283:446–451

Chen A-H, Liu S-C, Chen C-Y, Chen C-Y (2008) Comparative adsorption of Cu(II), Zn(II), and Pb(II) ions in aqueous solution on the crosslinked chitosan with epichlorohydrin. J Hazard Mater 154: 184–191

Chen J, Hao Y, Chen M (2014) Rapid and efficient removal of Ni 2+ from aqueous solution by the one-pot synthesized EDTA-modified magnetic nanoparticles. Environ Sci Pollut Res 21:1671–1679

Dinu MV, Dragan ES (2010) Evaluation of Cu2+, Co2+ and Ni2+ ions removal from aqueous solution using a novel chitosan/clinoptilolite composite: kinetics and isotherms. Chem Eng J 160:157–163

Galhoum AA, Mahfouz MG, Atia AA, Abdel-Rehem ST, Gomaa NA, Vincent T, Guibal E (2015) Amino acid functionalized chitosan magnetic nanobased particles for uranyl sorption. Ind Eng Chem Res 54:12374–12385

Ge H, Hua T, Chen X (2016) Selective adsorption of lead on grafted and crosslinked chitosan nanoparticles prepared by using Pb 2+ as template. J Hazard Mater 308:225–232

Giacometti JA, Job AE, Ferreira FC (2005) Thermal analysis of chitosan based networks. Carbohydr Polym 62:97–103

Guibal E, Guzman J, Navarro R, Ruiz M, Sastre A (2004) Influence of the speciation of metal ions on their sorption on chitosan

He J, Lu Y, Luo G (2014) Ca(II) imprinted chitosan microspheres: an effective and green adsorbent for the removal of Cu(II), Cd(II) and Pb(II) from aqueous solutions. Chem Eng J 244:202–208

Hosseini F, Sadighian S, Hosseini-Monfared H, Mahmoodi NM (2016) Dye removal and kinetics of adsorption by magnetic chitosan nanoparticles. Desalin Water Treat 57:24378–24386

Hritcu D, Dodi G, Silion M, Popa N, Popa MI (2011) Composite magnetic chitosan microspheres: in situ preparation and characterization. Polym Bull 67:177–186

Hu X-J, Wang J-S, Liu Y-G, Li X, Zeng G-M, Bao Z-L, Zeng X-X, Chen A-W, Long F (2011) Adsorption of chromium (VI) by ethylenediamine-modified cross-linked magnetic chitosan resin: isotherms, kinetics and thermodynamics. J Hazard Mater 185:306–314

Huang L, Yuan S, Lv L, Tan G, Liang B, Pehkonen SO (2013) Poly(methacrylic acid)-grafted chitosan microspheres via surface-initiated ATRP for enhanced removal of Cd(II) ions from aqueous solution. J Colloid Interface Sci 405:171–182

Jarup L (2003) Hazards of heavy metal contamination. Br Med Bull 68: 167–182

Jeon BH, Dempsey BA, Burgos WD, Royer RA, Roden EE (2004) Modeling the sorption kinetics of divalent metal ions to hematite. Water Res 38:2499–2504

Jiang W, Wang W, Pan B, Zhang Q, Zhang W, Lv L (2014) Facile fabrication of magnetic chitosan beads of fast kinetics and high capacity for copper removal. ACS Appl Mater Interfaces 6:3421–3426

Kharissova OV, Dias HVR, Kharisov BI (2015) Magnetic adsorbents based on micro- and nano-structured materials. RSC Adv 5:6695–6719

Kim HR, Jang JW, Park JW (2016) Carboxymethyl chitosan-modified magnetic-cored dendrimer as an amphoteric adsorbent. J Hazard Mater 317:608–616

Li B, Jia D, Zhou Y, Hu Q, Cai W (2006) In situ hybridization to chitosan/magnetite nanocomposite induced by the magnetic field. J Magn Magn Mater 306:223–227

Li A, Lin R, Lin C, He B, Zheng T, Lu L, Cao Y (2016a) An environment-friendly and multi-functional absorbent from chitosan for organic pollutants and heavy metal ion. Carbohydr Polym 148: 272–280

Li R, Li P, Cai J, Xiao SJ, Yang H, Li AM (2016b) Efficient adsorption of both methyl orange and chromium from their aqueous mixtures using a quaternary ammonium salt modified chitosan magnetic composite adsorbent. Chemosphere 154:310–318

Lin HY, Sun T, Xue SF, Jiang XL (2016) Heavy metal spatial variation, bioaccumulation, and risk assessment of *Zostera japonica* habitat in the Yellow River estuary, China. Sci Total Environ 541:435–443

Lin CY, Li SX, Chen M, Jiang R (2017) Removal of Congo red dye by gemini surfactant C-12-4-C-12 center dot 2Br-modified chitosan hydrogel beads. J Dispers Sci Technol 38:46–57

Liu Y, Zheng YA, Wang AQ (2010) Enhanced adsorption of methylene blue from aqueous solution by chitosan-g-poly (acrylic acid)/vermiculite hydrogel composites. J Environ Sci 22:486–493

Lu S, Li HP, Zhang FR, Du N, Hou WG (2016) Sorption of Pb(II) on carboxymethyl chitosan-conjugated magnetite nanoparticles: application of sorbent dosage-dependent isotherms. Colloid Polym Sci 294:1369–1379

Luo X, Zeng J, Liu S, Zhang L (2015) An effective and recyclable adsorbent for the removal of heavy metal ions from aqueous system: magnetic chitosan/cellulose microspheres. Bioresour Technol 194: 403–406

Men HF, Liu HQ, Zhang ZL, Huang J, Zhang J, Zhai YY, Li L (2012) Synthesis, properties and application research of atrazine Fe 3 O 4 @SiO 2 magnetic molecularly imprinted polymer. Environ Sci Pollut Res 19:2271–2280

Mi FL, Wu SJ, Chen YC (2015) Combination of carboxymethyl chitosan-coated magnetic nanoparticles and chitosan-citrate complex gel beads as a novel magnetic adsorbent. Carbohydr Polym 131:255–263

Ngah WSW, Fatinathan S (2010) Adsorption characterization of Pb(II) and Cu(II) ions onto chitosan-tripolyphosphate beads: kinetic, equilibrium and thermodynamic studies. J Environ Manag 91:958–969

Peng S, Meng H, Ouyang Y, Chang J (2014) Nanoporous magnetic cellulose–chitosan composite microspheres: preparation, characterization, and application for Cu(II) adsorption. Ind Eng Chem Res 53: 2106–2113

Podzus PE, Daraio ME, Jacobo SE (2009) Chitosan magnetic microspheres for technological applications: preparation and characterization. Phys B Condens Matter 404:2710–2712

Prakash N, Sudha PN, Renganathan NG (2012) Copper and cadmium removal from synthetic industrial wastewater using chitosan and nylon 6. Environ Sci Pollut Res 19:2930–2941

Reddy DH, Lee SM (2013) Application of magnetic chitosan composites for the removal of toxic metal and dyes from aqueous solutions. Adv Colloid Interf Sci 201-202:68–93

Ruthven DM (1984) Principles of adsorption & adsorption processes. Wiley

Singh KP, Mohan D, Sinha S, Tondon GS, Gosh D (2003) Color removal from wastewater using low-cost activated carbon derived from agricultural waste material. Ind Eng Chem Res 42:1965–1976

Varma AJ, Deshpande SV, Kennedy JF (2004) Metal complexation by chitosan and its derivatives: a review. Carbohydr Polym 55:77–93

Wang JL, Chen C (2014) Chitosan-based biosorbents: modification and application for biosorption of heavy metals and radionuclides. Bioresour Technol 160:129–141

Wang Y, Li B, Zhou Y, Jia D (2008) Chitosan-induced synthesis of magnetite nanoparticles via iron ions assembly. Polym Adv Technol 19: 1256–1261

Wang Y, Li B, Zhou Y, Jia D (2009) In situ mineralization of magnetite nanoparticles in chitosan hydrogel. Nanoscale Res Lett 4:1041–1046

Wang Y, Li B, Zhou Y, Jia D, Song Y (2011) CS-Fe(II,III) complex as precursor for magnetite nanocrystal. Polym Adv Technol 22:1681–1684

Wang J, Xu W, Chen L, Huang X, Liu J (2014) Preparation and evaluation of magnetic nanoparticles impregnated chitosan beads for arsenic removal from water. Chem Eng J 251:25–34

Yuwei C, Jianlong W (2011) Preparation and characterization of magnetic chitosan nanoparticles and its application for Cu(II) removal. Chem Eng J 168:286–292

Zhou L, Wang Y, Liu Z, Huang Q (2009) Characteristics of equilibrium, kinetics studies for adsorption of Hg(II), Cu(II), and Ni(II) ions by thiourea-modified magnetic chitosan microspheres. J Hazard Mater 161:995–1002

Zhu Y, Hu J, Wang J (2014) Removal of Co2+ from radioactive wastewater by polyvinyl alcohol (PVA)/chitosan magnetic composite. Prog Nucl Energy 71:172–178